

Fatigue Assessment of Notched Steel Including Residual Stresses Obtained by the Rolling Process

G. Nicoletto¹ and A. Saletti²

Abstract: Fatigue strengthening of fillets by deep rolling is finding increased application for example in engine crankshaft production for functional and economical reasons. A fatigue design method aimed at exploiting the residual stresses that develop at a notched part following the rolling process is proposed. It is based on the superposition of residual stresses obtained by elastic-plastic FE simulation of the rolling process and the cyclic elastic stresses within a Haigh diagram framework. The fatigue design method is assessed using the experimental evidence obtained by testing notched specimens made of 30NiCrMo12 steel subjected to different rolling process parameters.

Keywords: Fatigue, residual stress, notch, Q&T steel, deep rolling, finite element.

1 Introduction

The fatigue design of mechanical parts containing notches is a classical problem that has been extensively treated in the past in textbooks. Notches are important structural details because often define the critical section where service stresses tend to be most severe. On the other hand, notches in mechanical parts cannot be entirely eliminated because of their functional motivation. Established approaches have emerged in the technical literature that account for both the local geometry and material structure via stress concentration factors, notch sensitivity factors, stress gradient etc.. Nicholas (2007) provides an up-to-date treatment of the problem.

Residual stresses are known to greatly affect fatigue strength of metals. Therefore, technological treatments are deliberately applied to mechanical parts to induce residual stresses and therefore to significantly improve their fatigue strength, see Rottger, Wilcke and Altenberger (2004). Besides thermo-chemical treatments, such as nitriding, case carburizing etc., mechanical treatments, such as rolling and

¹ Dept. of Industrial Engineering, University of Parma, Parma, Italy

² TP Engineering srl, Parma, Italy

shot peening, can strengthen notched metallic parts subjected to fatigue loading. The selection and implementation of such surface treatments for optimal strength improvement follow traditionally a trial-and-error approach rather than explicit calculation.

The crankshaft of internal combustion engines is a key mechanical component that is typically notch-strengthened. The crankshaft geometry is characterized by a sequence of pins separated by connecting webs. Due to overall engine size limitations, a small radius at the web-to-pin fillet locations of the crankshaft is often used. Since it is subjected to high cycle fatigue loading during its service life, the stresses at these high stress concentration locations could initiate fatigue cracks leading to catastrophic failure. From the design stand point, the stress analysis of a crankshaft is increasingly performed with the finite element method (FEM) because the complex geometry and multiple loading conditions can be readily incorporated into the computational model, see Henry, Toplosky and Abramczuk (1992).

Deep rolling technology is increasingly applied to crankshaft shoulder fillets by many car manufacturers for functional and economical motivations, see Altenberger (2005). Fillet deep rolling introduces compressive residual stresses on the contact surface and sub-surface, which prohibit fatigue cracks to initiate and continuously propagate. The aim of the present study is the development and assessment of a fatigue design approach for crankshafts, which, during their production, are subjected to a deep rolling treatment of the pin-to-web fillets, see Diefenbach, Hanselka, Berger and Wuttke (2010). Fatigue design of crankshafts follows either the local stress approach to crack initiation prediction, for example see Dang Van, Flavenot and Le Douaron (1984) or the fracture mechanics approach to crack propagation prediction, for example see Taylor, Ciepalowicz, Rogers and Devlukia (1997).

Here the first approach is adopted while taking full advantage of rolling process simulation and being compatible with the modern FE-based fatigue post-processors in order to speed up the crankshaft design and development cycle and minimize costly experimental design validation. The procedure discussed here is organized in three steps: i) FE simulation of the notch rolling process, ii) FE stress analysis of the part and iii) fatigue assessment by stress superposition within the FKM norm framework, FKM Guideline (2003).

The necessary experimentation required to support the proposed design procedure and reported here was developed within strict time and cost constraints according to the following choices: i) the 30NiCrMo12 steel, typically used for crankshaft production, ii) multiple rolling process conditions of notched specimens to experimentally determine an optimal process, iii) a simplified notch geometry rather than a crankshaft section (i.e. notched specimen) and iv) a rotating bending loading rather than a combined bending /torsion load of a crankshaft. The experimental

evidence obtained with specimens is then used to assess the proposed three-step design approach.

2 Experimental activity

This section presents the experimental activity performed to provide evidence to guide and support the methodology development phase. The material and notched geometry is initially presented along with the rolling process applied to the specimens. The influence of rolling-induced residual stresses on the fatigue behavior is finally quantified.

2.1 Material and specimen geometry

The material used is the low alloy 30NiCrMo12 steel. The chemical composition is as follows: C= 0.31%, Ni=2.90%, Cr=0.80%, Mo=0.40%, Mn=0.65%, Si=0.28%, P and S<0.035%, Fe= balance . The experimental program began with the machining of approx 100 specimens for monotonic and fatigue testing starting from normalized 12-mm-dia commercial bars of 30NiCrMo12. The specimens were then quenched and tempered (Q&T) according to the following cycle: i) heating to T=890°C for t=2h followed by quenching in oil; ii) re-heating to T=620° for t=2h and final cooling in air to room temperature. The steel microstructure of Figure 1 shows the presence of sorbite, a typical structure of a Q&T steel, having a homogeneous and fine globular phase.

The tensile properties of Q&T 30NiCrMo12 were determined using four specimens in a servo-hydraulic MTS 810 testing machine. The following data are obtained: Young's modulus of elasticity $E = 206 \text{ GPa} \pm 1.9 \text{ GPa}$; yield stress $R_s = 1017 \text{ MPa} \pm 5 \text{ MPa}$; ultimate stress $R_m = 1118 \text{ MPa} \pm 4 \text{ MPa}$; elongation to rupture $A\% = 21.4\% \pm 0.2$, see Saletti (2011).

The notched specimen geometry to be rolled and tested in fatigue is shown in Figure 3. It is characterized by a U-shaped notch of radius $R = 4 \text{ mm}$ and a theoretical concentration factor $K_t = 1,21$ referred to the net section area of diameter $d = 6\text{mm}$. A set of 20 Q&T specimens was used to obtain the reference fatigue curve of the 30NiCrMo12 in the untreated state.

2.2 Rolling of specimens and fatigue testing

Three sets of notched specimens were subjected to three different rolling treatments. The scheme of Figure 3 shows a specimen mounted between the two forming rolls of the rolling machine. One roll is free to rotate about its fixed axis while the second, opposing roll can be moved toward the first applying a prescribed force. The applied force controls the penetration depth of the forming rolls into the

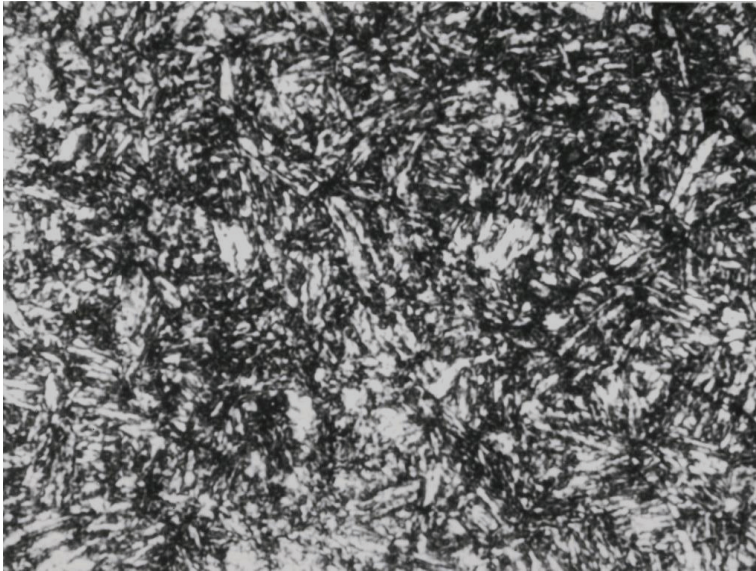


Figure 1: Microstructure of Q&T 30NiCrMo12 steel

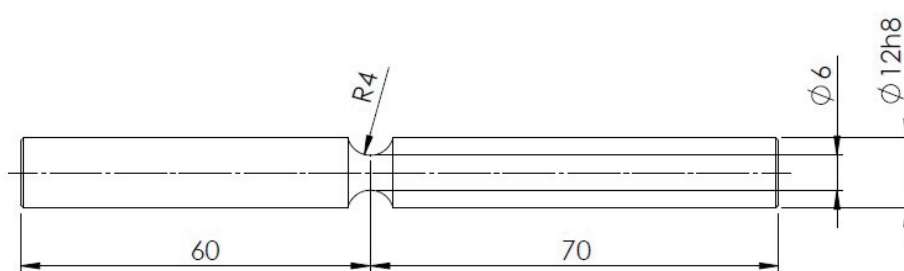


Figure 2: Specimen geometry (dimensions in mm)

notched specimen. The rolling process consists of simultaneous rolling and rotation of the specimen by friction of the co-rotating rolls while the rolling force is gradually increased to its maximum value. Such a force is maintained for a prescribed number of turns then it is gradually reduced to zero. The plastic deformation of the surface layer of the specimen results into a residual compressive stress system in the notch section, which will be discussed in a subsequent section. The three sets of specimens (approx 20 specimens each) were rolled to three different rolling forces, namely 4.5 kN, 8.0 kN e 9.0 kN, based on previous experience. The specimens underwent seven full rotations (i.e. each surface point underwent 14 passes).

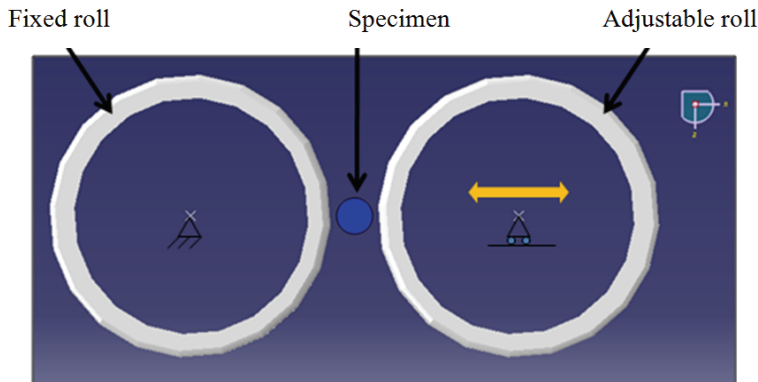


Figure 3: Scheme of the rolling process machine (in blu is specimen cross section)

After rolling, the 30NiCrMo12 specimens were tested under rotating cantilever bending machine (i.e. stress ratio $R = -1$) with multiple test stations (i.e. up to 8) at a frequency of 50 Hz and at room temperature. The S-N fatigue curves were determined following a statistical method described in JSME 002 standard (1981). It determines the 50% failure probability S-N curve of a material using a minimum of 14 specimens, i.e. eight for the slope section of the S-N curve, which is also called the finite fatigue life region (all specimens failed at a number of cycles N_f in the range $5 \times 10^4 - 10^7$ cycles), and at least six specimens for the endurance limit. The sloping section of the S-N curve is evaluated by linear regression of the (net nominal stress amplitude, cycles to failure) data for four stress amplitude levels. The standard deviation of the stress amplitude is then used as the step size to evaluate the fatigue limit following a reduced staircase method.

The plot of Figure 4 summarizes the experimental data and the four S-N curves for the 30NiCrMo12 in the untreated and notched state and for the three rolled conditions. The fatigue limits change from 332 MPa for the untreated state to higher values in the presence of rolling treatment. Namely, 478 MPa for $F = 4.5$ kN, 574 MPa for 8.0 kN and 456 MPa for 9.0 kN. It is found the intermediate rolling force (i.e. 8 kN) results in the highest fatigue limit improvement.

The differing slopes of the S/N portions of the fatigue curves may indicate different fatigue damage mechanisms as a function of the rolling process. The largest fatigue strength increment with respect to the untreated state is ca. 75%. Improvements of this kind are reported in the literature, see Altenberger (2005), where it is also pointed out that the improvement increases with tensile strength and notch severity.

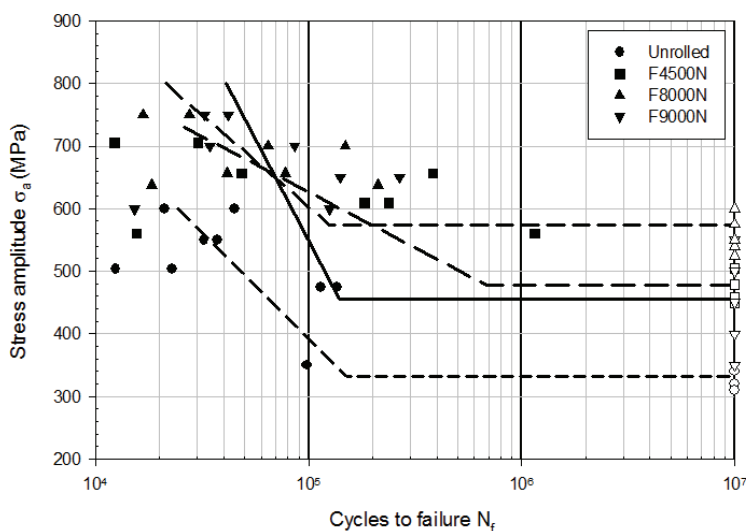


Figure 4: Experimental data and S/N curves for notched steel specimens in the untreated and rolled states (material 30NiCrMo12, open symbols: multiple run-out). The stress is computed referring to the net section.

Selected fracture surfaces were examined in the microscope and in the SEM. Crack initiation occurred on the surface for all specimens although differences were observed between the untreated and the rolled specimens.

3 Rolling process simulation

The fatigue assessment methodology proposed here rests on the preliminary prediction of the residual stresses in the notch region due to the rolling process by simulation. The presentation of phase is organized into three subsections: 1) determination of the constitutive law of the 30NiCrMo12 steel; 2) 3D FE model development of the rolling process; 3) determination of the residual stresses in specimens subjected to three different rolling conditions.

3.1 Constitutive law of 30NiCrMo12 steel

The determination of the material constitutive law to be used in the FE code is critical for predictive accuracy of the residual stresses. Because the rolling process produces severe plastic deformation due to cyclic contact stresses, see Bhargava, Hahn and Rubin (1985), a constitutive model that simulates the cyclic elastic-plastic behavior of the material is needed. Differently from previous works here

the simulation determines residual stresses due to the cyclic rolling process and not just a static contact analysis of a rigid roller on a surface. A nonlinear kinematic – isotropic hardening model based on the work of Lemaitre and Chaboche (2005) is chosen to correctly simulate both the cyclic behavior (e.g. Bauschinger effect) and the yield stress variation with cyclic loading (i.e. hardening /softening behavior). The kinematic component is associated to the translation of center of the yield surface, while the isotropic component describes the expansion of the yield surface. The kinematic component of this combined model, Lemaitre and Chaboche (2005), is given by

$$\dot{\alpha}_k = C_k \frac{1}{\sigma_0} (\sigma - \alpha) \dot{\bar{\varepsilon}}^{pl} - \gamma_k \alpha_k \dot{\varepsilon}^{pl} \quad (1)$$

where σ is the nodal stress, $\dot{\bar{\varepsilon}}^{pl} = \sqrt{\frac{2}{3} \dot{\varepsilon}^{pl} : \dot{\varepsilon}^{pl}}$ is the equivalent plastic strain rate, $\dot{\alpha}_k$ is the rule of the k-th yield surface translation, σ_0 is the yield surface radius (i.e. associated to the isotropic component of the combined model and calibrated to describe cyclic yielding behavior) and $\alpha = \int_{k=1}^N \alpha_k$, is the total *back-stress* (i.e. the sum of all k-th displacement of the yield surface center). C_k e γ_k are the two material parameters that are obtained from the monotonic stress-plastic strain ($\sigma_i; \varepsilon^{pl}$) curve. Integration of eq.(1) leads to

$$\alpha_k = \frac{C_k}{\gamma_k} (1 - e^{-\gamma_k \cdot \varepsilon^{pl}}), \quad (2)$$

where the unknowns, C_k e γ_k , are obtained by curve fitting.

The engineering stress-strain curve of Figure 5 demonstrates the presence of marked reduction of area prior to failure. Considering that severe plastic deformation are associated to elastic-plastic contact, a method was developed to obtain the true stress - true strain curve of the 30NiCrMo12 steel also shown in Figure 5, Saletti A., (2011). The behavior is almost bilinear with a strain to rupture of more than 90% and a rupture stress of 1680 MPa. The kinematic component of the elastic-plastic constitutive law of the material was inserted point-by-point in the ABAQUS code, Abaqus (2010).

The isotropic component of the Lemaitre-Chaboche model describes the expansion or reduction of the yield surface radius depending on the cyclic hardening/softening behavior. The calibration of this component was obtained by performing controlled cyclic elastic-plastic deformation tests on uniaxial tensile specimens using a servo-hydraulic testing machine MTS 810 equipped with a 10kN load cell and a high sensitivity extensometer. Cyclic push/pull tests with fixed $\pm \varepsilon (\Delta \varepsilon = 2\varepsilon)$ provide sets of ($\sigma_i^0; \bar{\varepsilon}_i^{pl}$) data. In the present experiments the 30NiCrMo12 steel was determined to cyclically soften as shown in Figure 6 where only the first and the seventh

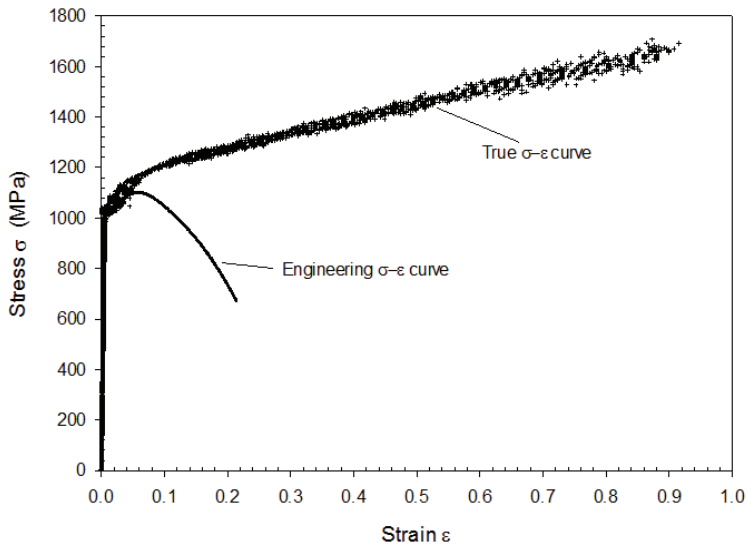


Figure 5: Stress-strain curves of 30NiCrMo12 steel.

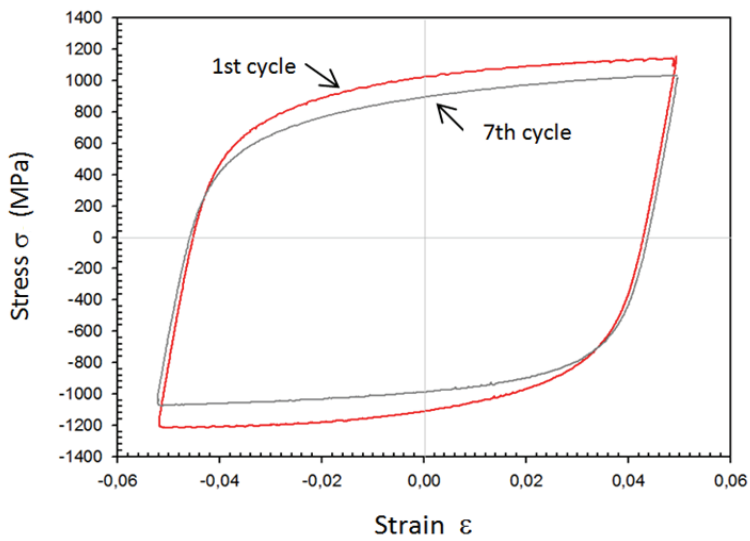


Figure 6: Cyclic hysteresis loops of 30NiCrMo12 steel.

hysteresis loops are plotted with experimental evidence of cyclically softening behavior (i.e. the yield surface in a two-dimensional plane $\sigma_1 - \sigma_2$ progressively reduces in size). Interestingly, the cyclic material behavior show a rapid stabilization after the first few cycles. The strain softening data with increasing number of cycles of 30NiCrMo12 were manually inserted in tabular form according to ABAQUS theory manual.

3.2 FE modeling of the rolling process

This section introduces the FE model development for the rolling process simulation and then presents the main results of the elastic-plastic rolling deformation. The simulation of the rolling process began with the development of the 3D FE model of the notched specimen geometry, see Figure 7. Suitable grading of element size and type (i.e. hexahedral solid elements) in view of the severe strain gradients associated with elastic-plastic contact conditions and reasonable number of DOF (i.e. 13280 elements) for containing the computational burden were the guiding modeling considerations.

The rolling contact was modeled using ABAQUS code capabilities, see ABAQUS (2010). Figure 2 shows that the two opposing rigid forming rolls move in the radial direction and enter into contact with the specimen notch. The force applied by the forming rolls gradually increases to its prescribed value in one specimen rotation, then it is maintained for three complete specimen rotations and finally reduced to zero in another rotation. Details of the sequence of boundary conditions required to obtain convergence of the process simulation are not specified here for sake of brevity. The ABAQUS Explicit version was used with optimized settings such as kinematic split hourglass control, aspect ratio etc., see Saletti (2011).

The 3D stress and strain fields at every step of the rolling process are obtained by FE analysis. Here special attention is devoted to the residual stress distributions. Figure 8a shows a coordinate system centered at the notch useful to describe the surface residual stresses as a function of angle θ and radial position r . Three stress components are defined in the scheme of Figure 8a, although three other stress components, namely σ_z , τ_{zq} and τ_{zr} are connected to the third coordinate axis z . Evidence of these components will be clear in a following sections. Figure 8b shows the surface stress components as a function of θ that develop when the rolling force $F_r = 8.0$ kN is applied and then removed. The stress σ_q is found to be largest of all the stress components and compressive. The max σ_q is at an angle of about 37 degrees and reaches -600 MPa. Considering that the rolling process is applied to influence the fatigue behavior, quite relevant is also the stress $\sigma_q = -300$ MPa at the minimum specimen cross-section.

The discussion of the typical process simulation data continues with the stress dis-

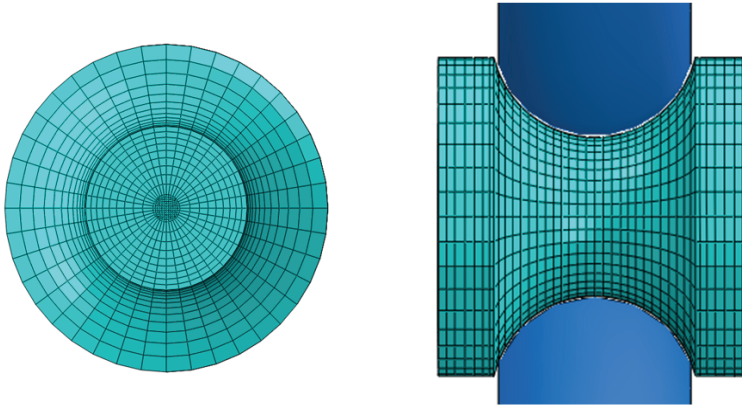


Figure 7: FEM model of the specimen and forming rolls

tribution in the minimum cross section (i.e. $\theta = 0^\circ$) shown in Figure 8c. Again, especially relevant is the evolution within the specimen section of the σ_q component. It is observed that it starts at the surface at -300 MPa, remains compressive and reaches -500 MPa at 1/6 of the section radius. Then becomes zero at 1/3 and then positive in the center of the specimen to maintain global equilibrium in the axial direction.

The complexity of the residual stress development process makes it almost impossible an experimental validation of the computed stresses. The x-ray diffraction method could in principle quantify the surface residual stresses although the small specimen size, severe stress gradient and surface curvature make the application challenging. Experiments with this technique are currently under way and will be reported in a future contribution.

A qualitative assessment of the present modeling capability is presented in Figure 9, where the residual equivalent plastic strain at the end of the rolling process are in Figure 9a. Figure 9b shows a detail of the surface and cross section of the specimen with evidence of residual shear strain (i.e. γ_{rz}), which is a 3D feature that depends on the number of passes and on the rolling contact force. Figure 9c shows the notch cross-section of a rolled specimen after metallographic preparation and chemical etching (i.e. Nital 2%). The picture shows a surface layer where etching shows severe deformation of the microstructure according to flow lines in analogy with the tilting of element sides due to shear straining in the Figure 9b. Furthermore, such structural banding disappears at some depth where the microstructure assumes the typical random appearance. It can be concluded that the rolling process appears realistically modeled by the present FE-based approach.

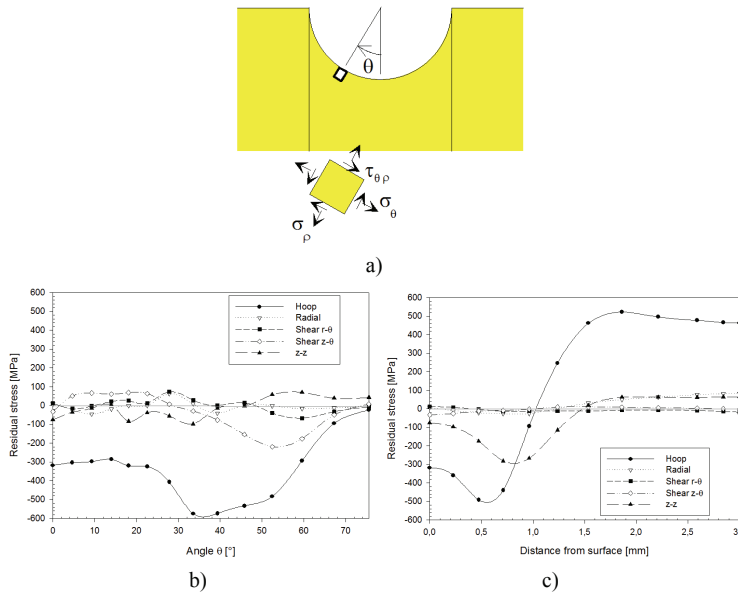


Figure 8: a) Coordinate system and residual stresses after rolling b) on the notch surface and c) below the free surface for $\theta = 0^\circ$ ($F_r = 8 \text{ kN}$; Mat. 30NiCrMo12)

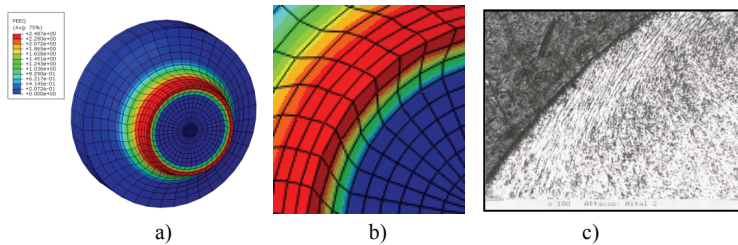


Figure 9: a) Residual plastic deformation after rolling b) detail showing the surface deformed FE layer c) surface layer microstructure of rolled 30NiCrMo12 ($F_r = 8.0 \text{ kN}$)

3.3 Residual stresses for fatigue assessment

The computed residual stresses generated by the three rolling forces applied to the fatigue specimens presented in a previous section are now discussed in relation to their influence on the fatigue assessment methodology. Since experimental evidence demonstrated that fatigue cracking develop at the minimum specimen

cross-section, (i.e. perpendicular to the cyclic principal stress), the attention is concentrated here on the axial stress component (with respect to the specimen axis i.e. σ_q with $q = 0$ in Figure 8a) as a function of the depth from the surface. This residual stress component is the most important because it is parallel to the bending stress applied to the specimen during fatigue testing.

Figure 10 shows the influence of the rolling force on the residual stress distribution below the surface. While the general trend is as expected (i.e. compressive near the free surface and tensile in the central part of the specimen), Figure 10 demonstrates that for the minimum rolling force ($F_r = 4.5$ kN) the stress peak is very near the surface and reaches a top value of -400 MPa, for the intermediate rolling force ($F_r = 8.0$ kN) the stress peak of about -500MPa develops at a depth of 0.5 mm from the surface and for the largest rolling force ($F_r = 9.0$ kN) the stress peak is even higher (i.e. 580MPa) and deeper into the specimen (i.e. 0.8 mm). On the other hand, the free surface residual stresses decrease with increasing rolling force from about - 400 MPa to about - 200MPa. The experimental evidence of the previous section demonstrated that the highest fatigue strength improvement is associate to the intermediate rolling force, indicating that neither the maximum residual stress level nor the surface residual stress value correlate with the fatigue strength improvement.

The value of the present FE-based simulation is the possibility of investigating process variants that optimize the residual stress distribution. In general, a notch rolling process has a large number of variables, (i.e. mechanical, geometrical, operative etc.). The present study has investigated only the rolling force magnitude, while roll geometry, notch geometry, material, number of specimen rotations, friction coefficient were kept constant.

Figure 11 shows the evolution of the axial stress of a point on the surface during the force application, the sequence of constant force roll passes and the final force decrease. Quite interestingly the residual stress associated to the minimum rolling force ($F_r = 4.5$ kN) does not increase during rolling except at the final unloading. The residual stress behavior for the intermediate rolling force ($F_r = 8.0$ kN) and for the largest rolling force ($F_r = 9.0$ kN) is quite similar with a gradual increase from -400 MPa to -500 MPa with repeated passes. At the end of the process the residual stress significantly decrease from the maximum values (especially for the largest rolling force case).

These calculations strongly depend on the constitutive law of the material, which here was experimentally obtained and calibrated. However, it can be stated that the rolling process finds in the simulation approach a powerful optimization tool.

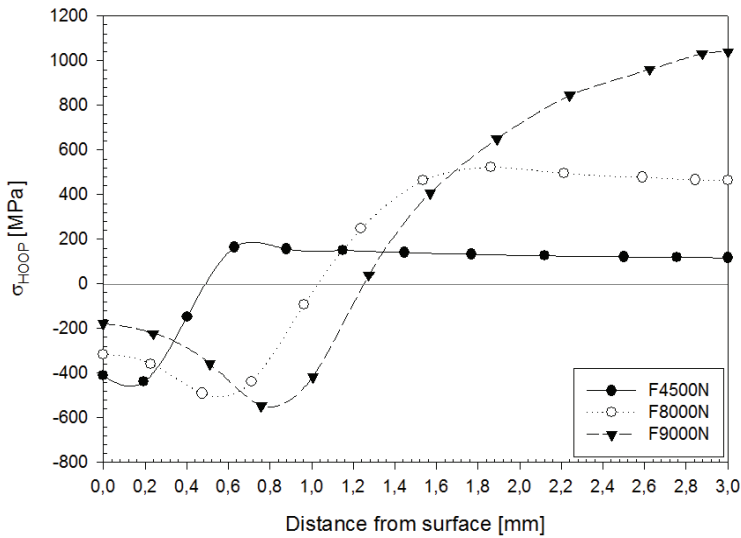


Figure 10: Residual stress distribution in the specimen cross-section as a function of the rolling force (Mat. 30NiCrMo12; 14 passes)

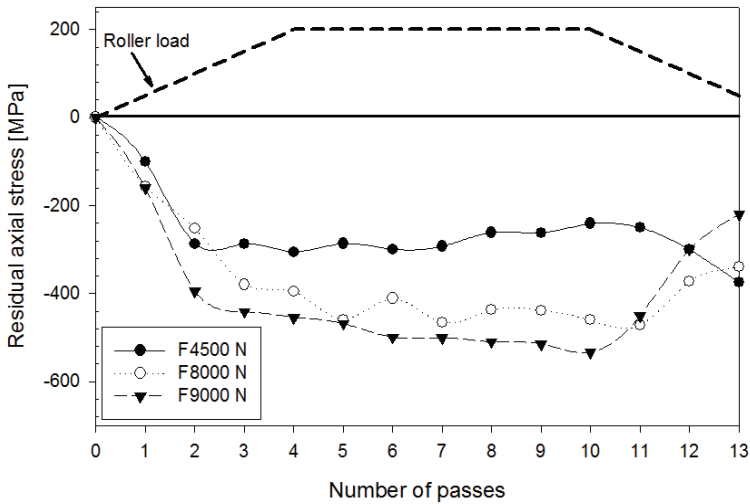


Figure 11: Evolution of the axial residual stress at the notch during the rolling process

4 Notch fatigue assessment in the presence of residual stresses

Initially the basic concepts adopted to treat the notch sensitivity in fatigue are applied to the present 30NiCrMo12 in the un-rolled state. Then, computed elastic notch stresses and residual stresses obtained by simulation are combined to predict the influence of the rolling process on notch fatigue strength of 30NiCrMo12. Finally, the fatigue strength predictions vs. the experimental evidence are discussed.

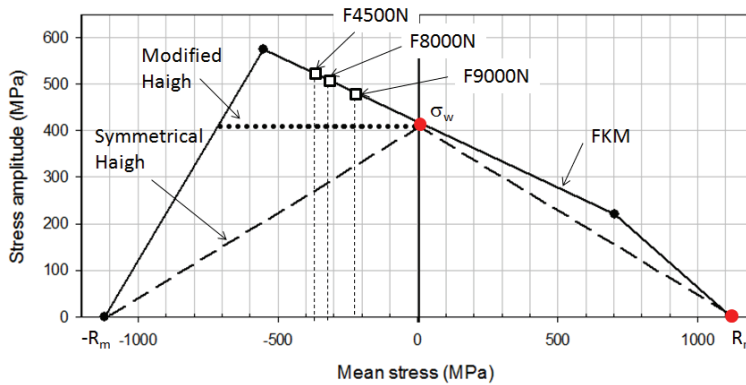


Figure 12: Haigh diagrams with the 50% failure probability fatigue limit envelope for notched 30NiCrMo12 and fatigue strengths estimates for the three rolling treatments

5 Residual stress effect on fatigue

Application of cyclic stresses may alter the residual stresses induced in the specimens by the rolling treatment. The stress level, however, should be high enough that plastic or micro-plastic deformation redistribute the peak compressive stresses. Since the present study deals with the long-life fatigue behavior of rolled specimens, stress amplitudes are assumed to be sufficiently low that residual stresses are unaffected. Under this assumption residual stresses are taken as a mean stress superposed to the variable-load-induced stress cycling. The experiments discussed here are associated to a fully reversed cyclic loading due to rotating bending (i.e. stress ratio $R = -1$) and to a uniaxial stress state. Therefore, use of the Haigh diagram to account to mean stress effects is the straightforward approach on the basis of the following data: local fatigue limit of the notched material under rotating bending load in the unrolled condition, (i.e. $\sigma_w = K_t \sigma_{w0} = 402$ MPa) and the ultimate tensile strength of the material (i.e. $R_m = 1110$ MPa). Most of the textbooks, however, either consider a Haigh diagram symmetrical about the y-axis or asymmetrical with

a horizontal line for negative mean stresses (i.e. the fatigue strength is not affected by a compressive residual stress) as depicted in Fig. 12.

No influence of a compressive residual stress on fatigue limit would be predicted. Therefore, a third Haigh diagram was introduced in Figure 12 using the FKM Guidelines (2003). This last Haigh diagram will be used in the next section to predict the influence of a residual stress due to the rolling process.

5.1 Prediction of the fatigue strength after rolling

The FKM-based Haigh diagram for a notched specimen geometry and the 30NiCrMo12 steel is now used to predict the increase in fatigue strength as a function of the rolling process using the computed residual stress as a mean stress.

Figure 13 shows the elastic bending stress distribution and the simulated residual stress distribution obtained by process simulation, respectively. A FE data post processing routine has been developed to automatically collect data at corresponding nodes, compute mean stress and stress amplitude and plot data of interest in the Haigh diagram.

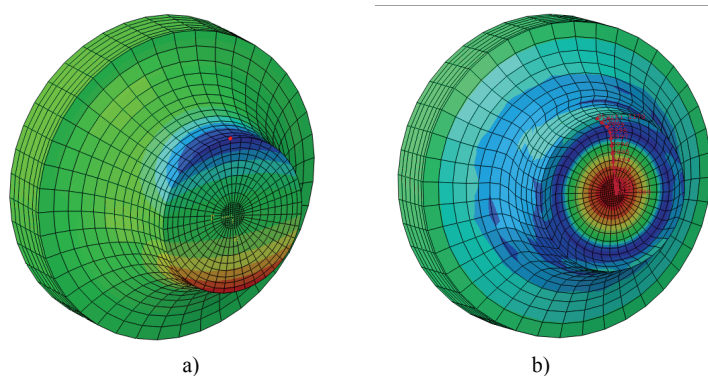


Figure 13: a) axial stress due to specimen bending; b) axial residual stress after notch rolling ($F_r = 9.0$ kN)

The Haigh diagram of Figure 12 shows as open squares the 50% probability local notch fatigue strength estimates for the following surface residual stresses: -374MPa for a rolling force $F=4.5$ kN, -338MPa for $F=8$ kN and -220 MPa for $F=9$ kN. Several observations can be made: i) an estimate of the fatigue strength in the presence of a residual stress is associated to the intersection of the surface residual stress and the upper limit line of the Haigh diagram. ii) small differences are obtained for the first two rolling force levels and a lower fatigue strength for the

maximum rolling force; iii) a maximum theoretical fatigue strength (i.e. -580MPa) is associated to a surface residual stress reaching about -560 MPa.

A direct correlation of the estimated notch fatigue strength including the influence of rolling residual stresses for the 30NiCrMo12 steel and the experimental data obtained with the experimental activity described in a previous section is obtained with the plot of Figure 14. Apparently, the present approach is capable of revealing a fatigue strength improvement associated to the rolling treatment. Its straightforward application assumes fatigue crack initiation at the free surface avoiding more complex fracture mechanics based concepts such as fatigue crack propagation threshold, residual stress intensity factor etc. On the other hand, this approach tend to considerably underestimate (more than 30%) the potential benefit of a notch rolling treatment. Unfortunately, such underestimate is highest for optimal rolling condition demonstrated by experiment.

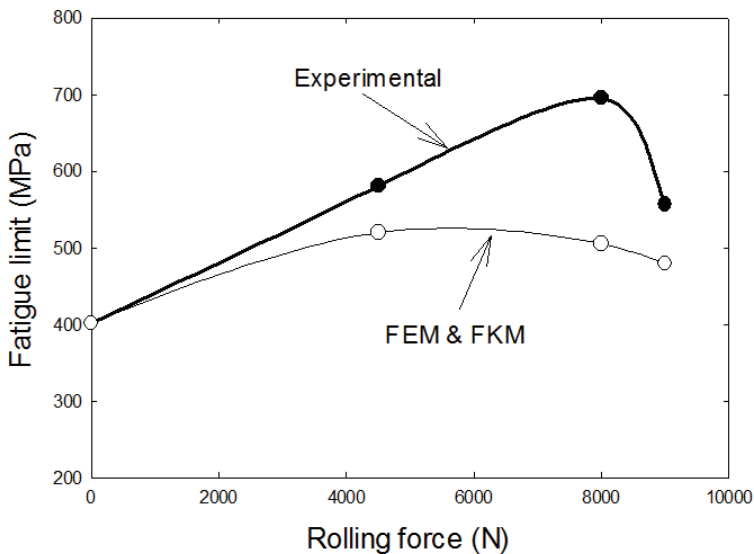


Figure 14: Predicted vs. experimental dependence of the local 50% failure probability fatigue limit on the notch rolling force

The relative simplicity of the proposed method and its reasonable predictive accuracy makes it suitable for fatigue design of crankshafts subjected to a deep rolling treatment of the pin-to-web fillets. Its applicability using full scale fatigue tests is under investigation.

6 Conclusions

A fatigue design procedure aimed at exploiting the residual stresses that develop at a notch following the elastic-plastic rolling process has been proposed and applied to a simple test case. The following conclusions are reached:

The three steps procedure consisting of i) FE simulation of the notch rolling process, ii) elastic FE stress analysis of the notched part and iii) automated fatigue assessment by stress superposition in a Haigh diagram, has been applied to a notch geometry made 30NiCrMo12 steel subjected to rotating bending with reasonable success.

1. Validation of the procedure was possible because extensive experimentation was carried out in order to determine basic material parameters and fatigue strengths under controlled rolling conditions.
2. The procedure can be readily extended to the deep rolling of crankshaft fillets thus speeding up part development cycle and minimize costly experimental design validation.

References

- ABAQUS** (2010): *Analysis user manual*, volume III, HKS, Pawtucket USA 2010.
- Altenberger, I.** (2005): Deep Rolling: The Past The Present and The Future, *Procs ICSP9*, 145-155.
- Bhargava V., Hahn G.T., Rubin C.A.** (1985): Elastic-plastic finite element model of rolling contact—part 1: analysis of single contacts, *J Appl Mech Trans ASME*;52:67–74.
- Bhargava V., Hahn G.T., Rubin C.A.** (1985): Elastic-plastic finite element model of rolling contact—part 2: analysis of repeated contacts, *J Appl Mech Trans ASME*; 52:75–82.
- Dang Van K., Flavenot J.F., Le Douaron A.** (1984): Critere d’amorçage en fatigue a grand nombre de cycles sous sollicitations multiaxiales. *J Comm Fatigue Soc Franc Metall*, RE1123.
- Diefenbach C., Hanselka H., Berger C., Wuttke U.** (2010): Experimentelle Untersuchungen zur Schwingfestigkeit festgewalzter Stahlkurbelwellen, *Automobil-technische Zeitschrift* : ATZ 3, No.2, pp.54-58
- FKM-Guideline** (2003): *Analytical Strength Assessment*, 5th edition, 2003, English Version.
- Henry J., Toplosky J., Abramczuk M.** (1992): Crankshaft durability prediction

— a new 3-D approach, *SAE Paper 920087*. Warrendale (PA): Society of Automotive Engineers.

JSME S002 (1981): *Standard Method of Statistical Fatigue Testing* (JSME S 002), Japan Society of Mechanical Engineers.

Lemaitre, J., Chaboche, J.L. (2005): *Mechanics of Solid Materials*. Cambridge University Press, London.

Nicholas T. (2006): *High cycle fatigue- A mechanics of material approach*, Elsevier.

Rottger K., Wilcke G., Altenberger I. (2004): *Leichtbau und Betriebsfestigkeit*, Munchen, 2004, p. 293.

Saletti A. (2011): Fatigue strength prediction of deep rolled crankshafts, M.S. Thesis, University of Parma, (in Italian).

Taylor D., Ciepalowicz A.J., Rogers P., Devlukia J. (1997) Prediction of fatigue failure in a crankshaft using the technique of crack modeling, *Fatigue Fract Eng Mater Struct*; 20:13–21.